Solid-State ^{31}P NMR Chemical Shielding Tensors in Phosphonates and Bisphosphonates: A Quantum Chemical Investigation

Yong Zhang and Eric Oldfield*

Departments of Chemistry and Biophysics, University of Illinois at Urbana−Champaign, 600 South Mathews Avenue, Urbana, Illinois 61801

Received: April 8, 2004

We report the results of a quantum chemical investigation of the ^{31}P nuclear magnetic resonance (NMR) isotropic chemical shieldings (σ_{iso}) and the ^{31}P NMR chemical shielding tensor principal values (σ_{ii}, $i = 1-3$) in a series of eight different phosphonates, including the bisphosphonates pamidronate and risedronate currently in use in bone resorption therapy. We used primarily Hartree−Fock methods with a 6-311++G(2d,2p) basis set and the CSGT (continuous set of gauge transformations) formalism to predict the experimental observables, using various approaches to incorporating intermolecular, crystal lattice effects. Good predictions of the ^{31}P NMR isotropic chemical shielding, shielding tensor principal values, and tensor orientations were obtained, with $R^2 = 0.95$ and ∼7% root-mean-square error from experiment. In the zwitterionic aminophosphonates, electrostatic (lattice) interactions were found to be strong but could be well accounted for by incorporating charge lattice effects into the calculations. The ability to now predict both isotropic and anisotropic shielding (shift) tensors in phosphonates and bisphosphonates should open the way to the determination of their protonation states when bound to proteins, information which is not accessible from crystallographic studies.

Introduction

Phosphonates and bisphosphonates are important inhibitors of isoprene biosynthesis and have considerable therapeutic importance.[1,2] For example, the bisphosphonates pamidronate (Aredia), alendronate (Fosamax), risedronate (Actonel), and zoledronate (Zometa) are currently used to treat a variety of bone resorption diseases, such as osteoporosis, Paget's disease, and hypercalcemia. Bisphosphonates, as well as monophosphonates,[2] can also kill a variety of protozoan parasites,[3,4] responsible for diseases such as malaria, sleeping sickness, and the leishmaniases, and some stimulate the $\gamma\delta$ T cells of the immune system to kill tumor cells and bacterial pathogens.[5,6] There is thus considerable interest in determining the precise enzyme inhibition mechanisms caused by such drugs, and here, it seems likely that solid-state ^{31}P NMR methods may provide useful information, since both isotropic and anisotropic chemical shifts (or shieldings) are expected to be highly sensitive to protonation state (as they are in, e.g., carboxylic acids[7]).

In previous work, there have been a number of studies of ^{31}P shifts in phosphates and other molecular systems, including some ab initio calculations.[8−21] However, there have been no reports of ^{31}P shift/shielding tensor predictions for phosphonates or bisphosphonates. The ability to accurately predict these properties should be of importance since it should facilitate determination of the protonation states of these species when bound to a variety of enzymes, which can be expected to facilitate the drug design process. We thus report in this article our initial investigations of the correlations between ^{31}P NMR shielding properties and structure, using a combination of experimental and quantum chemical methods.

Experimental Section

Experimental Aspects. Solid-state ^{31}P magic-angle sample-spinning (MAS) NMR spectra of the zwitterionic form of risedronate[22] were obtained at 145.8 MHz (corresponding to a ^{1}H NMR resonance frequency of 360 MHz) using a "home-built" 8.45 T spectrometer and at 303.6 MHz using a Varian Inova 750 MHz instrument. Spectra were recorded with and without proton-decoupling at a variety of spinning speeds, and the spinning sideband intensities were analyzed by using the Herzfeld−Berger method,[23] as implemented in the MBA program,[24] to obtain δ_{ii} values. The ^{31}P NMR chemical shift reference was external 85% H_3PO_4.

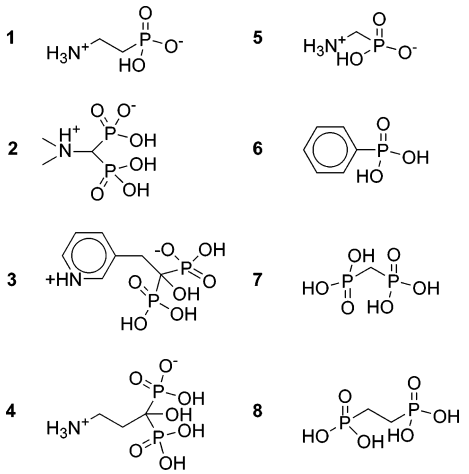

Figure 1. Structures of the phosphonates and bisphosphonates investigated.

Computational Aspects. We used the Gaussian 98 program[25] to compute the chemical shielding tensors of two model systems (PO_4^{3-} and HPO_4^{2-}) plus eight molecular systems (**1**−**8**) whose structures are shown in Figure 1. The geometries used were those reported crystallographically.[22,26−35] We tested numerous different theoretical methods: Hartree−Fock (HF), density functional theory (DFT, using a variety of pure and hybrid

10.1021/jp040281n CCC: $27.50
Published on Web 11/19/2004

functionals),[36−40] and a series of different basis sets (through 6-311++G(3df,3pd)) together with the use of CSGT (continuous set of gauge transformations),[41] GIAO (gauge independent atomic orbitals),[42] and IGAIM (a slight variation on CSGT)[43] methods. The use of the HF method with a 6-311++G(2d,2p) basis and the CSGT method gave good results for both model systems (Table S1 in the Supporting Information) as well as for **1**−**8**, with no obvious improvements with the use of DFT methods, which were always highly correlated with the HF results (Figures S1 and S2). GIAO results are provided in the Supporting Information (Table S2). IGAIM results are the same as CSGT results.

In addition to calculations on isolated molecules, we also investigated crystal lattice effects using molecular clusters and charge field perturbation.[44] In the first method, additional molecules were clustered around the central molecule of interest, using known crystal structures to define the locations of the added molecules. In the second method, the additional molecules were represented by point charges, rather than by real atoms.[45,46] We also used a combination of both methods, as discussed below. The charge lattices for each crystal structure were generated by using the Shelxtl program.[47] We investigated the use of both Mulliken and natural population analysis (NPA)[48] charges, plus the electrostatic potential (ESP) derived charges in Gaussian 98: MK (Merz−Kollman),[49] Chelp,[50] ChelpG,[51] ESPDipole,[25] and AtomDipole.[25]

Most calculations were performed on Silicon Graphics (Mountain View, CA) O-200, O-300, and O-2000 computers, using up to 16 processors. In a few cases, GIAO calculations with charge field perturbation were also carried out by using the PQS program[52] (a new version of the Texas-90 program used previously[45] for calculating ^{13}C chemical shielding tensors) using a PQS (PQS Inc., Fayetteville, AR) workstation with 12 processors.

Results and Discussion

Isolated Molecules. The results of a single-crystal ^{31}P NMR study of **1** have been reported,[10] making it a good test case for ^{31}P shielding tensor predictions in phosphonates. Based on the results of our initial model compound studies (Table S1), we used the HF/6-311++G(2d,2p)/CSGT method using the reported crystallographic structure of **1** and obtained the σ_{ii} values shown in Table 1. As may be seen in Table 1, the experimental δ_{ii} and predicted σ_{ii} values are highly correlated, with $R^2 \sim 0.98$, Table S3. We then investigated the tensor orientation using the icosahedral tensor representation approach introduced by Alderman et al.,[53] obtaining the results shown in Table 2 (and Table S4, for the GIAO method). For χ_i prediction, we again found that the HF/6-311++G(2d,2p) results were highly correlated with experiment, with $R^2 > 0.93$. There were, however, deviations in the slopes from the ideal value of −1.00, for both δ_{ii} and χ_i (Table S3). In principle, these could be due to basis/functional deficiencies or to the lack of incorporation of an essential "ingredient" in the calculations: electrostatic field effects. We return to this topic later.

We next investigated the ^{31}P NMR results for the seven other compounds shown in Figure 1 (**2**−**8**), including the bisphosphonates risedronate (**3**) and pamidronate (**4**) currently in use in bone resorption therapy. In three of the eight molecules, there is only one type of protonation pattern present, while in the other five molecules, there are two crystallographically nonequivalent phosphonate groups, which raises the question as to their specific assignments. For **8**, the experimental shifts are the same for both sites, so there is no assignment question. Since we show below in more detail that the experimental δ_{iso}, δ_{ii}, and χ_i results for the unambiguously assigned phosphorus sites can be reproduced with good accuracy, we therefore used the results of our calculations to make chemical shift assignments for the other species.

Based on the $\delta_{iso}/\sigma_{iso}$ correlations shown in Figure 2A (CSGT) and Figure S3A (GIAO), the absolute shielding of 85% H_3PO_4 is predicted to be ∼357 ppm, about a 30 ppm deviation from the value reported by Jameson et al.[20b] of 328.35 ppm. However, the R^2 is still quite promising: 0.84 (Figure 2A). The major outliers in the predicted σ_{iso} are all found to be associated with the negatively charged sites, as illustrated by the open circle data points shown in Figures 2A and S3A. This effect is reminiscent of that seen previously with the carboxylate groups in threonine and tyrosine[45] and can be largely corrected for by incorporation of crystal lattice effects, as discussed below. The correlations between the computed and experimental principal values (Figures 2B and S3B) are also good ($R^2 > 0.93$), but as shown in Table S5, the slopes of ca. −1.8 and the absolute

TABLE 1: ^{31}P NMR Shielding Results Using the CSGT Method

compd	structure[a]	method[b]	σ_{11}/δ_{11}[c] (ppm)	σ_{22}/δ_{22}[c] (ppm)	σ_{33}/δ_{33}[c] (ppm)	$\sigma_{iso}/\delta_{iso}$[c] (ppm)
1		expt[10]	87.1	15.6	−47.5	18.4
	AMEPAC[27]		229.5	330.5	470.6	343.6
2		expt[8,11]	70	19	−62	9.1
			79	0	−67	3.9
	SOPSAR[31]		220.1	320.8	498.6	346.5
			252.9	318.3	474.6	348.6
3		expt[d]	74.5	36.4	−42.6	22.8
			85.2	7.9	−42.8	16.8
	[22]		272.5	296.8	434.4	334.6
			220.0	332.2	470.7	341.0
4		expt[8]	83	6	−41	15.9
			77	16	−54	12.8
	SOPSEV[31]		255.9	310.0	460.2	342.0
			224.7	318.6	500.8	348.0
5		expt[8]	97	21	−64	18.3
	AMEPOS[26]		223.4	321.1	501.7	348.7
6		expt[9]	69	22	−28	21.0
	BZPHOT[30]		258.0	303.6	455.1	338.9
7		expt[9]	74	32	−27	26.2
			71	32	−30	24.7
	MEYDPA[34]		252.8	291.5	449.4	331.2
			263.0	285.7	455.3	334.7
8		expt[9]	63	51	−16	32.7
			63	51	−16	32.7
	EDPHAC10[35]		253.7	283.6	438.6	325.3
			253.7	283.6	438.6	325.3

[a] The Cambridge crystal structural database IDs are given for compounds **1**, **2**, and **4**−**8**. For **3**, the crystal structure of the monohydrate was used because the NMR measurements were performed on the same sample. The structural references are given in superscripts. [b] The experimental references are given in superscripts. In case of different measurements for a compound in the literature, the most precise data are cited here. [c] Values are the experimental δ_{ii} and computational σ_{ii} data, respectively. [d] This work.

TABLE 2: ^{31}P NMR Shielding Tensors for 1 in the Icosahedral Representation[a] (CSGT)

charge	χ_1 (ppm)	χ_2 (ppm)	χ_3 (ppm)	χ_4 (ppm)	χ_5 (ppm)	χ_6 (ppm)
expt[b]	−0.8	43.5	−34.4	76.5	8.9	16.6
none	341.1	307.2	442.6	239.3	354.9	324.5
MK	342.4	320.2	398.3	261.8	350.4	331.6
NPA	343.3	321.5	395.8	263.9	350.5	332.2
AtomDipole	348.2	316.6	383.7	266.9	340.6	339.3

[a] The unit for χ is ppm (see refs 46 and 53 for the computational details of the icosahedral tensor elements). The experimental and computational χ_i results were calculated by using the experimental shift and computational shielding values, respectively. [b] Reference 10.

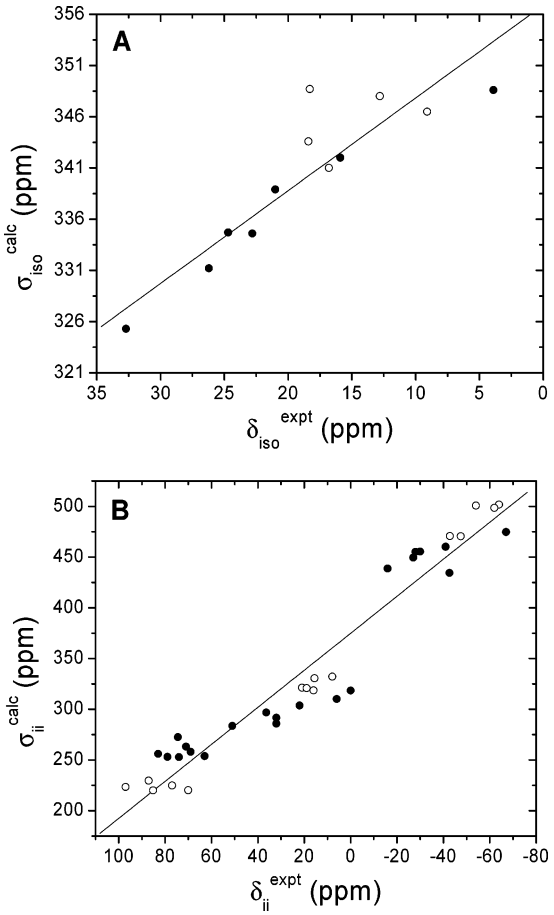

Figure 2. Experimental versus computed ^{31}P NMR shielding results for (A) σ_{iso} (CSGT) and (B) σ_{ii} (CSGT). Solid and open circles represent data points for neutral and negatively charged phosphorus sites, respectively.

shieldings (of 85% H_3PO_4) clearly indicate some inadequacies in these initial calculations. Based on our previous results with threonine and tyrosine,[45] it seemed likely that omission of crystal lattice (electrostatic field) effects might be compromising the accuracy (and precision) of these calculations, so we next investigated such effects in **1**−**8**.

Crystal Lattice Effects on ^{31}P NMR Shieldings. There are two basic approaches for introducing neighboring group interactions into chemical shielding tensor calculations:[44] cluster models and charge field perturbation (CFP) effects. The advantage of using the cluster approach is that one can, at least in principle, dissect different intermolecular interactions explicitly. However, due to the high computational expense of using large clusters with large basis sets, this method generally employs only a single shell of molecular species that interact directly with the central molecule of interest, and even in this situation, sometimes only fragments of the interacting chemical species can be considered, restricting the method to short-range interactions. On the other hand, in the charge field perturbation approach, due to its low computational cost, much longer range interactions can be included, but there is no explicit consideration of the shorter range intermolecular interactions. Here, we consider the use of both of these methods individually, together with the use of both methods in combination, to see to what extent short- and long-range interactions might influence the ^{31}P NMR properties.

We first investigated compound **5**, since it has the largest absolute deviation from the correlation line (Figure 2A) when using isolated molecule computations alone. The CSGT results are shown in Table S6, and additional results with GIAO and on other phosphonates are shown in Table S7. For **5**, there are eight molecules that are hydrogen-bonded to the central molecule, based on its known crystal structure.[26] In our cluster calculations, these eight additional molecules were explicitly incorporated, as shown in Figure 3. We used a 6-311++G(2d,2p) basis for all directly hydrogen bonded heavy atoms, while for the rest of the atoms in the eight additional molecules, a 3-21G** basis was used. This resulted in a 1066 basis function calculation for this, the smallest aminophosphonate. As shown in Table S6, the CSGT cluster calculation gave some improvements in the predicted ^{31}P NMR properties; e.g., the deviation in σ_{iso} from the straight line shown in Figure 2A reduces from 8.5 to 2.3 ppm. This suggests that direct hydrogen bonding with the first shell of interacting species might play an important role in affecting their ^{31}P NMR properties, consistent with a previous study on phosphorylated amino acids.[14] Such calculations are, however, very lengthy, so we next investigated to what extent the far more rapid charge field perturbation method might influence the NMR shielding predictions.

To deduce an appropriate charge lattice size, we carried out a series of calculations on **5** using either MK or NPA charges with lattice spheres of 3.0, 4.0, 5.0, 7.5, 10.0, 12.5, and 15.0 Å radius. Atoms in the central molecule (**5**) were treated explicitly using a 6-311++G(2d,2p) basis, while atoms falling inside the lattice sphere were treated as point charges. As may be seen in Figure 4, the computed isotropic chemical shielding and the three principal values of the ^{31}P chemical shielding tensor all essentially converge at a radius of ∼7.5 Å. There is an oscillatory behavior seen with both σ_{iso} and σ_{ii} at short distances, which may be attributed to the "overcompensation" of the lattice effect when essentially only the nearest neighbor H^+ are included in the calculations (resulting in a large deshielding), but this effect is rapidly dampened out as more charges are added, and the results with the 7.5 Å lattice are about the same as those with the 15 Å lattice. This convergence behavior was found to be independent of the type of charges employed, as well as the molecules under investigation (see e.g. Tables S6 and S7). When compared with the computational results on isolated molecules, the σ_{ii} slopes improved, from −1.74 to −1.27 (−1.20), with $R^2 = 0.993$ (0.995), when using the MK (NPA) charge lattice scheme, and the absolute shielding predicted for 85% H_3PO_4 also improved, from 380.0 to 362.1 ppm (359.5 ppm).

We also tested a combined cluster/CFP approach on compound **5**. As shown in Table S6, using a charge lattice of 7.5 Å radius and restoring the hydrogen-bonded molecules around the phosphorus sites from point charges to real molecules (6-311++G(2d,2p) for the directly hydrogen bonded atoms and STO-3G for the others) resulted in similar predictions for σ_{iso} as with the cluster approach alone. Since using even larger basis sets for the additional cluster molecules is not practical (e.g., for compound **4**, even using STO-3G or 3-21G** for the hydrogen-bonded molecules would result in 1728 or 2944 basis functions, respectively), it seems unlikely that further improvements can be made by using the cluster approach. While other methods, such as the use of periodic boundary conditions, should also in principle be applicable in model systems, these methods would not be of any use in investigating bisphosphonates or phosphonates bound to the macromolecular targets of primary interest, proteins.

These improvements in property predictions with incorporation of a charge lattice are also well demonstrated by consideration of compound **1**, which has an accurate single-crystal

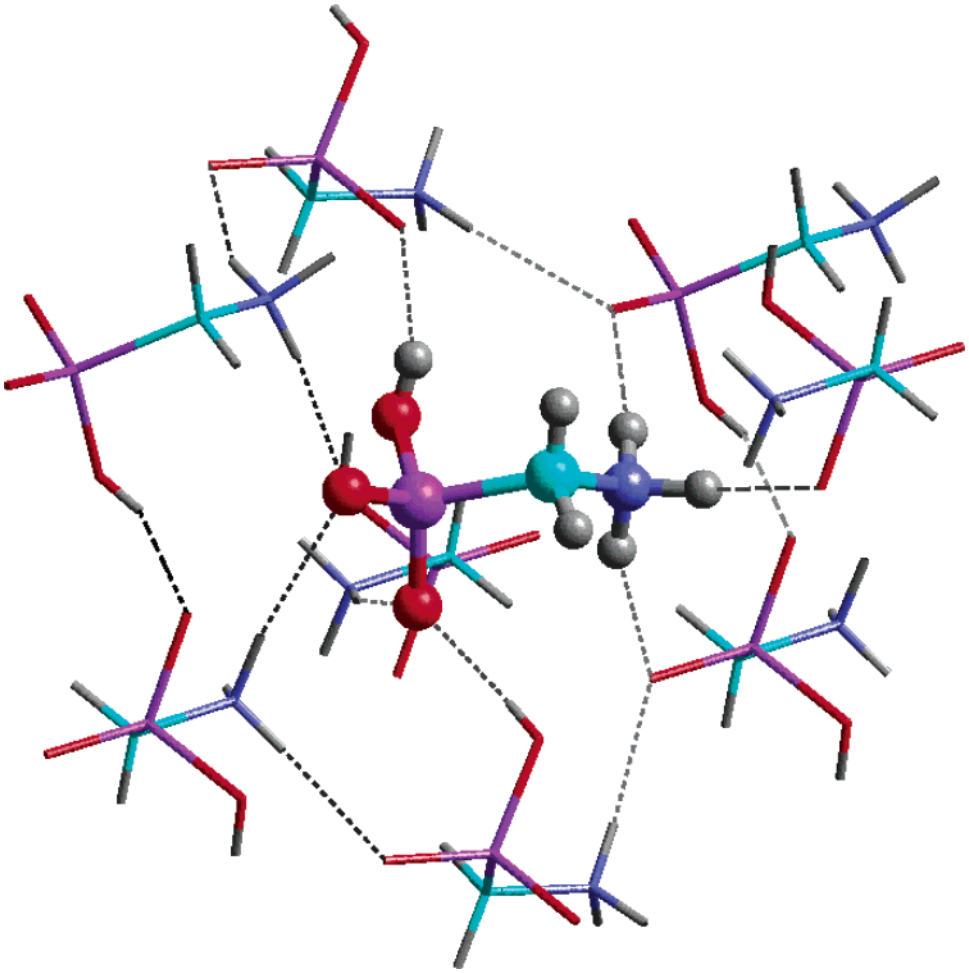

Figure 3. Cluster structure for compound **5** (ball and stick) surrounded by eight hydrogen-bonded molecules (cylinders) based on the crystal structure for **5** (ref 26). The atom color scheme is as follows: P = violet, C = cyan, N = blue, O = red, H = gray. The hydrogen bonds are illustrated by the dark dashed lines.

^{31}P NMR tensor determination reported.[10] For the principal values (σ_{ii}), the CFP approach clearly provides an improved performance over that found with the isolated molecule calculations. This can be seen in Table S3, in which the R^2 values obtained from the theory-versus-experiment correlations for σ_{ii} are essentially equal to the ideal value of 1.0. Moreover, the root-mean-square (rms) error in σ_{ii} greatly decreases: from 12.4 ppm (isolated molecule) to 1.6, 0.2, and 2.8 ppm, when using MK, NPA, and AtomDipole charges, respectively. The slope also reduces, from −1.78 (isolated molecule) to −1.19, −1.15, and −1.03, when using MK, NPA, and AtomDipole charge lattices, respectively. The icosahedral tensor components (Table 2) using the CFP approach also improve, as shown by their increased R^2 values, reduced rms errors, and improved slopes, again as shown in Table S3. The rms error for χ_i is now ∼6−9% of the experimental range (of 110.9 ppm) and the slopes are very close to the ideal value of −1.00. Thus, CSGT-HF/6-311++G(2d,2p) calculations with a 7.5 Å charge lattice yield very good correlations between theory and experiment for all three ^{31}P NMR properties.

As demonstrated by the results on compounds **1**, **4**, and **5** (see Table S7), calculations using other charge schemes, including Mulliken charges and other ESP-derived charge schemes, showed no further improvement over the above results, although in some calculations using AtomDipole charges, there was a slightly better range in the σ_{ii} values when compared with the experimental data. Full results for CSGT-HF/6-311++G(2d,2p) calculations using a 7.5 Å charge lattice with MK charges for all title compounds (**1**−**8**) are shown in Table 3, and those with NPA and AtomDipole charges in Table S2. Both neutral and negatively charged phosphorus sites (solid and open circle points, Figures 5 and S4) can be well predicted by using this approach. With MK charges, the rms errors between theory and experiment are found to be 2.1 ppm for σ_{iso} (equal to 7% of the whole σ_{iso} range of 29 ppm), half the error seen with the isolated molecule calculations, and the slope is −1.00 with an intercept of 356.0 ppm. For the ^{31}P NMR shielding tensor principal values, the use of MK charges yields $R^2 = 0.947$ and a 12.2 ppm rms error in δ_{ii}, or again a 7% rms error over the whole δ_{ii} range of 164 ppm, Table S5.

Not unexpectedly, simultaneously predicting both correct absolute shieldings as well as correct slopes remains a challenge. At present, we believe the most useful approach is to use the slope/intercept values from the $\delta^{expt}/\sigma^{calc}$ correlations to make small corrections to the predicted shifts, i.e., for the HF-CSGT/6-311++G(2d,2p)/MK method:

$$\delta_{iso}^{pred} = 356.0 - 1.00\sigma_{iso}^{calc} \quad (1)$$

$$\delta_{ii}^{pred} = 364.6 - 1.44\sigma_{ii}^{calc} \quad (2)$$

$$\chi_i^{pred} = 355.0 - 1.14\chi_i^{calc} \quad (3)$$

Using these three equations, we obtain the corrected shift prediction results shown in Figure 6. Here, we compare the

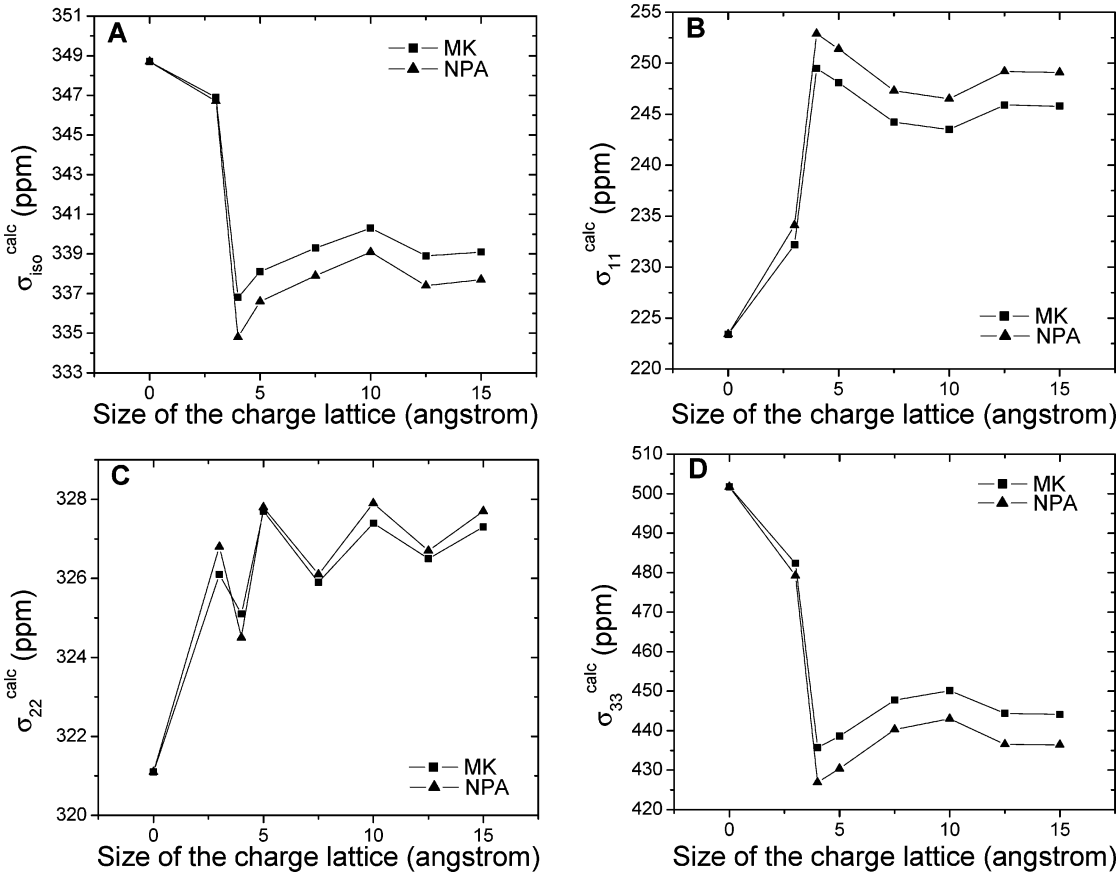

Figure 4. The effects of charge lattice size and charge population schemes on computed ^{31}P NMR shielding data for **5**, obtained from the CSGT calculations: (A) σ_{iso}; (B) σ_{11}; (C) σ_{22}; (D) σ_{33}.

TABLE 3: ^{31}P NMR Shielding Results from CSGT/MK CFP Calculations

compd	structure[a]	charge[b]	σ_{11}/δ_{11}[c] (ppm)	σ_{22}/δ_{22}[c] (ppm)	σ_{33}/δ_{33}[c] (ppm)	$\sigma_{iso}/\delta_{iso}$[c] (ppm)
1		expt[10]	87.1	15.6	−47.5	18.4
	AMEPAC [27]		256.3	338.8	416.1	337.1
2		expt[8,11]	70	19	−62	9.1
			79	0	−67	3.9
	SOPSAR [31]		233.4	325.3	475.3	344.7
			250.6	325.6	472.1	349.4
3		expt[d]	74.5	36.4	−42.6	22.8
			85.2	7.9	−42.8	16.8
	[22]		279.7	301.9	417.5	333.0
			249.9	342.1	421.9	338.0
4		expt[8]	83	6	−41	15.9
			77	16	−54	12.8
	SOPSEV[31]		263.0	323.0	442.1	342.7
			235.3	325.0	480.6	347.0
5		expt[8]	97	21	−64	18.3
	AMEPOS[26]		244.2	325.9	447.7	339.3
6		expt[9]	69	22	−28	21.0
	BZPHOT[30]		282.6	323.4	404.0	336.7
7		expt[9]	74	32	−27	26.2
			71	32	−30	24.7
	MEYDPA[34]		269.3	299.0	413.7	327.3
			277.3	298.4	419.8	331.9
8		expt[9]	63	51	−16	32.7
			63	51	−16	32.7
	EDPHAC10[35]		267.6	297.8	402.1	322.5
			267.6	297.8	402.1	322.5

[a] See Table 1 footnote a. [b] See Table 1 footnote b. [c] See Table 1 footnote c. [d] This work.

experimental versus predicted shifts and shift tensor elements (δ_i, δ_{ii}, and χ_i) obtained by using the CSGT-HF/6-311++G(2d,2p)/MK method for the three monophosphonates (**1**, **5**, and **6**) and one bisphosphonate (**8**, with two identical phosphorus sites and one experimental shift) whose assignments are unambiguous (solid circles, ●), superimposed on the values computed for the four bisphosphonates whose specific assignments are unknown (open circles, ○). Clearly, there is excellent accord between theory and experiment for the systems whose specific assignments are known unambiguously. These 5 δ_{iso}, 15 δ_{ii}, and 6 χ_i values have very small rms errors (Figure 6A−C) and R^2 values of 0.99, 0.98, and 0.95, respectively. This good accord between theory and experiment strongly supports the use of such quantum chemical methods in making spectral assignments when such information is not otherwise available.

^{31}P NMR Chemical Shielding Tensor Properties. Finally, we consider the ^{31}P NMR shielding tensors in more detail. There are two types of phosphorus site in the phosphonates studied here: one is neutral with two hydroxyl groups, $-PO(OH)_2$, while the other has one formal negative charge, with one of the two hydroxyl groups being deprotonated, $-PO(OH)O^-$. In accord with these general features, the computational results predict two basic sets of ^{31}P NMR shielding tensor orientations and principal values. Among the 13 phosphorus sites investigated, 5 have negatively charged (deprotonated) hydroxyl groups: **1**, **5**, and one of the two sites in compounds **2**, **3**, and **4**. In these systems, the O═P−O$^-$ group has been shown crystallographically[22,26−28,31] to contain two almost equal P−O bond lengths (O═P═O)$^-$. In all of these five sites, as exemplified in Figure 7A, the most shielded component (σ_{33}) is approximately along the O═P═O or O−O vector, σ_{22} approximately bisects the O═P═O angle, and the most deshielded component (σ_{11}) is perpendicular to the (O═P═O)$^-$ plane.

The remaining eight phosphorus sites are neutral ($-P(O)(OH)_2$). The P═O bond has more electron density than the P−OH bond,

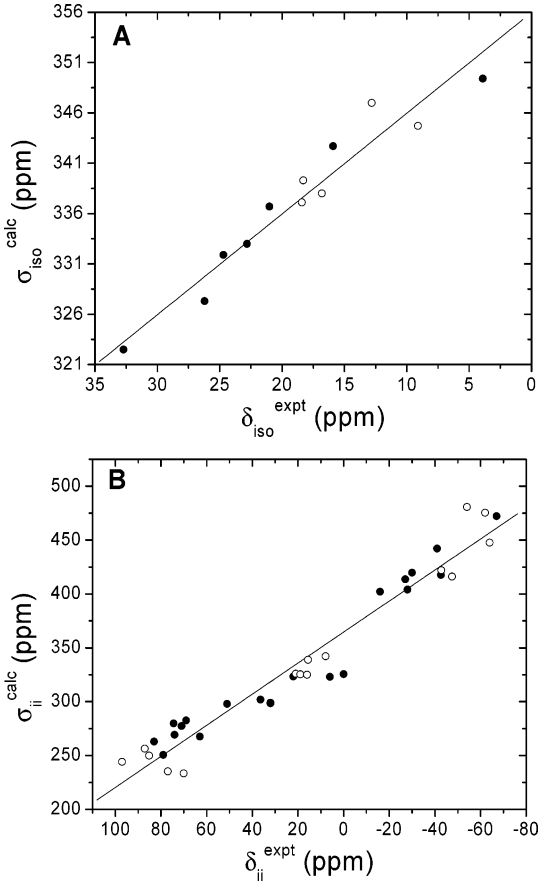

Figure 5. CSGT/MK charge lattice computational results for ^{31}P NMR isotropic chemical shieldings (A) and shielding tensor principal values (B). The solid and open circles represent neutral and negatively charged phosphorus sites, respectively.

and for these neutral sites, the most shielded component (σ_{33}) now lies close to the P═O bond vector. The plane that contains the two less shielded components (σ_{22} and σ_{11}) is of course perpendicular to σ_{33} and is very close to the plane of the two P−OH bonds, as shown in Figure 7B. In this type of site, σ_{11} lies approximately along the bisector of the two P−OH bonds, while σ_{22} is approximately parallel to the vector connecting the two oxygen atoms in the hydroxyl groups. Only in the case of compound **8** are these two deshielded components reversed. In this compound, the difference between the experimental results for δ_{22} and δ_{11} is only 12 ppm, while for all other neutral phosphorus sites with the same pattern, this difference is always >40 ppm. The origin(s) of this effect are not known.

In addition to these differences in shielding tensor orientations, there are also differences in the magnitudes of the average σ_{ii}/δ_{ii} values between the protonated ($-PO(OH)_2$) and deprotonated ($-PO(OH)O^-$) phosphonate groups. The average experimental δ_{ii} values for the neutral species are 72.1, 28.8, and −33.5 ppm (for δ_{11}, δ_{22}, and δ_{33}), while in the deprotonated species the corresponding values are, on average, 83.3, 15.9, and −54.1 ppm. On conversion from $-PO(OH)_2$ to $-PO(OH)O^-$, both δ_{22} and δ_{33} become more shielded while δ_{11} becomes more deshielded. These correlations can be seen in the experimental results, Figure S5. Figure S5A shows the correlation between δ_{11} and δ_{33}, Figure S5B δ_{11} and δ_{22}, and Figure S5C δ_{22} and δ_{33}. The correlation coefficient $|R|$ values vary from 0.66 to 0.75. These correlations originate primarily from intramolecular effects, since they are present in the single-molecule calculation results shown in Figures S5D−F, where $|R|$ values range from 0.76 to 0.82. The isotropic chemical shift

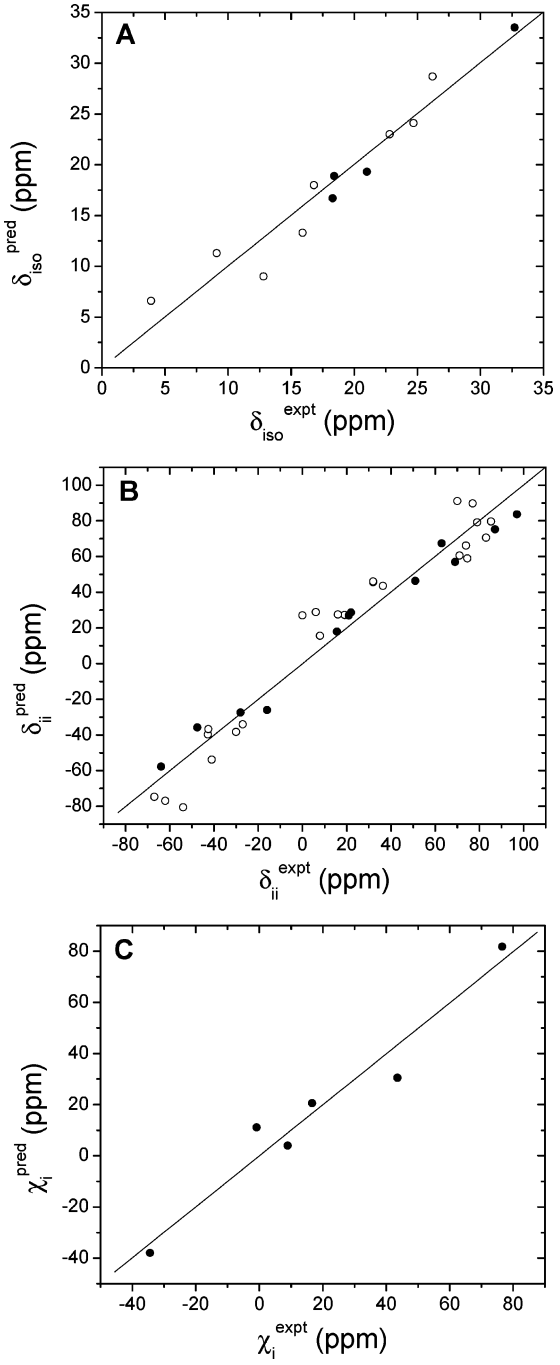

Figure 6. Experimental versus computational predictions for ^{31}P NMR properties: (A) δ_{iso}; (B) δ_{ii}; (C) χ_i. The solid and open circles are for sites with unambiguous assignments and tentative assignments (based on the HF calculations), respectively.

covers a total range of 29 ppm and is correlated with the average of the three P−O bond lengths, R_{PO}^{av}, as shown in Figure S6A and S6B ($|R| = 0.82$ and 0.81, respectively).

Conclusions

The results we have described above are of interest since they represent the most comprehensive study to date of the ^{31}P NMR chemical shielding tensors in a series of phosphonates and bisphosphonates, including molecules currently in clinical use. Both HF and DFT methods were found to have the potential for the quite accurate prediction of the solid-state ^{31}P NMR shielding tensor properties. Best accord with experiment was obtained when electrostatic field effects were incorporated into

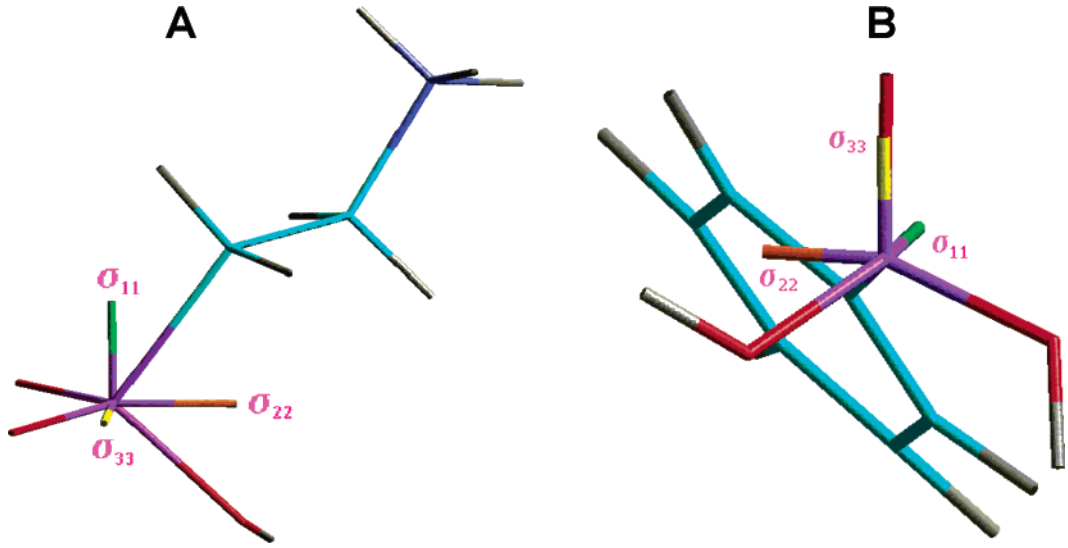

Figure 7. ^{31}P NMR chemical shielding tensor orientations in (A) **1** and (B) **6** obtained by using the CSGT/MK CFP approach. The atom coloring scheme is the same as in Figure 3. The tensor orientations are typical of monoanionic (A) or neutral (B) phosphonates.

the calculations, with δ_{iso}, δ_{ii}, and χ_i (after slope/intercept corrections) values being predictable within ~7% error versus experiment. The computational results also reveal that there are large tensor orientation differences between neutral and negatively charged phosphorus sites and that at least in **1**, these tensor orientation predictions are confirmed by experiment, giving further confidence in the utility of such calculations. When taken together, these results indicate that it should now be possible to predict both isotropic and anisotropic chemical shift (tensor) information in phosphonates and bisphosphonates with quite good accuracy. Combined with the use of ^{13}C and ^{15}N NMR shift results, this can be expected to be of particular use in deducing complete protonation state information for clinically important phosphonate and bisphosphonate drug molecules bound to their protein targets, information which cannot be deduced crystallographically.

Acknowledgment. This work was supported by the United States Public Health Service (NIH grant GM50694). Computations were carried out in part at the National Center for Supercomputing Applications (funded in part by the National Computational Science Alliance, Grant MCB-000020N). We thank Dr. Gary L. Meints and Junhong Mao for providing the risedronate results.

Supporting Information Available: Theoretical ^{31}P NMR shielding results of PO_4^{3-} and HPO_4^{2-} models (Table S1); ^{31}P NMR shielding results using GIAO, CSGT/NPA and CSGT/AtomDipole methods (Table S2); statistical results for ^{31}P NMR shielding calculations on **1** (Table S3); GIAO ^{31}P NMR shielding tensors for **1** in the icosahedral representation (Table S4); statistical results for ^{31}P NMR shielding calculations on phosphonates and bisphosphonates (Table S5); crystal field effects on computed ^{31}P NMR shieldings of **5** using the CSGT-HF/6-311++G(2d,2p) method (Table S6); computed ^{31}P NMR shielding results with the CFP approach (Table S7); HF vs B3LYP calculated ^{31}P NMR shielding tensor principal elements for HPO_4^{2-} and ^{31}P NMR isotropic shielding for PO_4^{3-} (Figure S1); plot of the computed ^{31}P NMR chemical shielding vs % HF exchange for HPO_4^{2-} using BPW91/6-311++G(2d,2p) (Figure S2); experimental vs computed ^{31}P NMR shielding results for σ_{iso} (GIAO) and σ_{ii} (GIAO) (Figure S3); experimental vs computed ^{31}P NMR shielding results for σ_{iso} (CSGT/NPA and CSGT/AtomDipole) and σ_{ii} (CSGT/NPA and CSGT/AtomDipole) (Figure S4); comparisons between δ_{ii}/σ_{ii} tensor elements for **1**−**8** (Figure S5); relationships between $\delta_{iso}/\sigma_{iso}$ and the average of three PO bond lengths for **1**−**8** (Figure S6). This material is available free of charge via the Internet at http://pubs.acs.org.

References and Notes

(1) Harada, S.; Rodan, G. A. *Nature* **2003**, *423*, 349−355.
(2) Jomaa, H.; Wiesner, J.; Sanderbrand, S.; Altincicek, B.; Weidemeyer, C.; Hintz, M.; Turbachova, I.; Eberl, M.; Zeidler, J.; Lichtenthaler, H. K.; Soldati, D.; Beck, E. *Science* **1999**, *285*, 1573−1576.
(3) Yardley, V.; Khan, A. A.; Martin, M. B.; Slifer, T. R.; Araujo, F. G.; Moreno, S. N.; Docampo, R.; Croft, S. L.; Oldfield, E. *Antimicrob. Agents Chemother.* **2002**, *46*, 929−931.
(4) Rodriguez, N.; Bailey, B. N.; Martin, M. B.; Oldfield, E.; Urbina, J. A.; Docampo. R. *J. Infect. Dis.* **2002**, *186*, 138−140.
(5) Wilhelm, M.; Kunzmann, V.; Eckstein, S.; Reimer, P.; Weissinger, F.; Ruediger, T.; Tony, H. P. *Blood* **2003**, *102*, 200−206.
(6) Wang, L.; Kamath, A.; Das, H.; Li, L.; Bukowski, J. F. *J. Clin. Invest.* **2001**, *108*, 1349−1357.
(7) Gu, Z. T.; McDermott, A. *J. Am. Chem. Soc.* **1993**, *115*, 4282−4285.
(8) Harris, R. K.; Merwin, L. H.; Hägele, G. *Magn. Reson. Chem.* **1989**, *27*, 470−475.
(9) Harris, R. K.; Merwin, L. H.; Hägele, G. *J. Chem. Soc., Faraday Trans.* **1989**, *85*, 1409−1423.
(10) Calsteren, M.-R. V.; Birnbaum, G. I.; Smith, I. C. P. *J. Chem. Phys.* **1987**, *86*, 5405−5410.
(11) Klose, G.; Trahms, L.; Möps, A. *Chem. Phys. Lett.* **1985**, *122*, 545−549.
(12) Asakawa, N.; Sato, D.; Sakurai, M.; Inoue, Y. *J. Phys. Chem. A* **2000**, *104*, 2716−2723.
(13) Alam, T. M. *Int. J. Mol. Sci.* **2002**, *3*, 888−906.
(14) Potrzebowski, M. J.; Assfeld, X.; Ganicz, K.; Olejniczak, S.; Cartier, A.; Gardiennet, C.; Tekely, P. *J. Am. Chem. Soc.* **2003**, *125*, 4223−4232.
(15) Tossell, J. A.; Lazzeretti, P. *J. Chem. Phys.* **1987**, *86*, 4066−4069.
(16) Tossell, J. A.; Lazzeretti, P. *Chem. Phys. Lett.* **1987**, *140*, 37−40.
(17) *Phosphorus 31 NMR*: *Principles and Applications*; Gorenstein, D. G., Ed.; Academic Press: Orlando, FL, 1984.
(18) Turner, G. L.; Smith, K. A.; Kirkpatrick, R. J.; Oldfield, E. *J. Magn. Reson.* **1986**, *70*, 408−415.
(19) Alam, T. M. In *Modelling NMR Chemical Shifts*; Facelli, J. C., de Dios, A. C., Eds.; ACS Symposium Series 732; American Chemical Society: Washington, DC, 1999; pp 320−334. Alam, T. M. *Ab Initio Calculation of Nuclear Magnetic Resonance Chemical Shift Anisotropy Tensors. 1. Influence of Basis Set on the Calculation of 31P Chemical Shifts*; Report No. SAND98-2053; Sandia National Laboratories: Albuquerque, NM, 1998.
(20) (a) Gierke, T. D.; Flygare, W. H. *J. Am. Chem. Soc.* **1972**, *94*, 7277−7283. (b) Jameson, C. J.; de Dios, A.; Jameson, A. K. *Chem. Phys. Lett.* **1990**, *167*, 575.

(21) Vyalikh, A. V.; Vorotolova, L. S.; Shchegolev, B. F. *Phosphorus, Sulfur Silicon* **2001**, *170*, 1−3.
(22) Gossman, W. L.; Wilson, S. R.; Oldfield, E. *Acta Crystallogr.* **2003**, *C59*, m33−m36.
(23) Herzfeld, J.; Berger, A. E. *J. Chem. Phys.* **1980**, *73*, 6021−6030.
(24) Eichele, K. *HBA*: *Graphical Herzfeld−Berger Analysis*, version 1.4.4; 2001.
(25) Frisch, M. J.; Trucks, G. W.; Schlegel, H. B.; Scuseria, G. E.; Robb, M. A.; Cheeseman, J. R.; Zakrzewski, V. G.; Montgomery, J. A., Jr.; Stratmann, R. E.; Burant, J. C.; Dapprich, S.; Millam, J. M.; Daniels, A. D.; Kudin, K. N.; Strain, M. C.; Farkas, O.; Tomasi, J.; Barone, V.; Cossi, M.; Cammi, R.; Mennucci, B.; Pomelli, C.; Adamo, C.; Clifford, S.; Ochterski, J.; Petersson, G. A.; Ayala, P. Y.; Cui, Q.; Morokuma, K.; Malick, D. K.; Rabuck, A. D.; Raghavachari, K.; Foresman, J. B.; Cioslowski, J.; Ortiz, J. V.; Stefanov, B. B.; Liu, G.; Liashenko, A.; Piskorz, P.; Komaromi, I.; Gomperts, R.; Martin, R. L.; Fox, D. J.; Keith, T.; Al-Laham, M. A.; Peng, C. Y.; Nanayakkara, A.; Gonzalez, C.; Challacombe, M.; Gill, P. M. W.; Johnson, B. G.; Chen, W.; Wong, M. W.; Andres, J. L.; Head-Gordon, M.; Replogle, E. S.; Pople, J. A. *Gaussian 98*, revision A.9; Gaussian, Inc.: Pittsburgh, PA, 1998.
(26) Darriet, M.; Darriet, J.; Cassaigne, A.; Neuzil, E. *Acta Crystallogr. B* **1975**, *31*, 469−471.
(27) Okaya, Y. *Acta Crystallogr.* **1966**, *20*, 712−715.
(28) Travnicek, Z.; Kasparek, F.; Marek, J.; Hendrych, J. *Acta Univ. Palacki. Olomuc.* **1996**, *35*, 43−48.
(29) Glowiak, T.; Sawka-Dobrowolska, W. *Acta Crystallogr. B* **1980**, *36*, 961−962.
(30) Weakley, T. J. R. *Acta Crystallogr. B* **1976**, *32*, 2889−2890.
(31) Shikol'nikova, L. M.; Sotman, S. S.; Afonin, E. G. *Kristallografiya* **1990**, *35*, 1442−1449.
(32) Neels, A.; Stoeckli-Evans, H.; Costisella, B.; Jancke, H.; Knudsen, K. D.; Pattison, P. *Helv. Chim. Acta* **1999**, *82*, 35−43.
(33) Kulpe, S.; Seidel, I.; Szulzewsky, K. *Cryst. Res. Technol.* **1984**, *19*, 669−674.
(34) DeLamatter, D.; McCullough, J. J.; Calvo, C. *J. Phys. Chem.* **1973**, *77*, 1146−1148.
(35) Peterson, S. W.; Gebert, E.; Reis, A. H.; Druyan, M. E.; Mason, G. W.; Peppard, D. F. *J. Phys. Chem.* **1977**, *81*, 466−471.
(36) Becke, A. D. *Phys. Rev. A* **1988**, *38*, 3098−3100.
(37) Perdew, J. P.; Burke, K.; Wang, Y. *Phys. Rev. B* **1996**, *54*, 16533−16539.
(38) Becke, A. D. *J. Chem. Phys.* **1993**, *98*, 5648−5652.
(39) Lee, C.; Yang, W.; Parr, R. G. *Phys. Rev. B* **1988**, *37*, 785−789.
(40) Adamo, C.; Barone, V. *J. Chem. Phys.* **1998**, *108*, 664−675.
(41) Cheeseman, J. R.; Frisch, M. J.; Trucks, G. W.; Keith, T. A. *J. Chem. Phys.* **1996**, *104*, 5497−5509.
(42) Ditchfield, R.; Hehre, W. J.; Pople, J. A. *J. Chem. Phys.* **1972**, *54*, 724−728.
(43) Keith, T. A.; Bader, R. F. W. *Chem. Phys. Lett.* **1992**, *194*, 1−8. Keith, T. A.; Bader, R. F. W. *Chem. Phys. Lett.* **1993**, *210*, 223−231.
(44) de Dios, A. C.; Oldfield, E. *Chem. Phys. Lett.* **1993**, *205*, 108−116.
(45) de Dios, A. C.; Laws, D. D.; Oldfield, E. *J. Am. Chem. Soc.* **1994**, *116*, 7784−7786.
(46) Arnold, W. D.; Sanders, L. K.; McMahon, M. T.; Volkov, A. V.; Wu, G.; Coppens, P.; Wilson, S. R.; Godbout, N.; Oldfield, E. *J. Am. Chem. Soc.* **2000**, *122*, 4708−4717.
(47) *Shelxtl Version 5.1*; Bruker AXS, 1998.
(48) Glendening, E. D.; Reed, A. E.; Carpenter, J. E.; Weinhold, F. *NBO*, version 3.1; Theoretical Chemistry Institute, University of Wisconsin: Madison, WI.
(49) Besler, B. H.; Merz, K. M., Jr.; Kollman, P. A. *J. Comput. Chem.* **1990**, *11*, 431−439.
(50) Chirlian, L. E.; Francl, M. M. *J. Comput. Chem.* **1987**, *8*, 894−905.
(51) Breneman, C. M.; Wiberg, K. B. *J. Comput. Chem.* **1990**, *11*, 361−373.
(52) *PQS*, version 2.4; Parallel Quantum Solutions: Fayetteville, AR. http://www.pqs-chem.com.
(53) Alderman, D. W.; Sherwood, M. H.; Grant, D. M. *J. Magn. Reson.* **1993**, *A101*, 188−197.